

Effective-mass theory for superlattices grown on (11 N)-oriented substrates

Jian-Bai Xia

Chinese Center of Advanced Science and Technology (World Laboratory), P.O. Box 8730, Beijing 100 080, China
and Institute of Semiconductors, Chinese Academy of Sciences, P.O. Box 912, Beijing 100 083, * China

(Received 16 July 1990; revised manuscript received 3 December 1990)

An effective-mass formulation for superlattices grown on (11 N)-oriented substrates is given. It is found that, for GaAs/Al $_x$ Ga $_{1-x}$ As superlattices, the hole subband structure and related properties are sensitive to the orientation because of the large anisotropy of the valence band. The energy-level positions for the heavy hole and the optical transition matrix elements for the light hole apparently change with orientation. The heavy- and light-hole energy levels at $\mathbf{k}_{\parallel}=\mathbf{0}$ can be calculated separately by taking the classical effective mass in the growth direction. Under a uniaxial stress along the growth direction, the energy levels of the heavy and light holes shift down and up, respectively; at a critical stress, the first heavy- and light-hole energy levels cross over. The energy shifts caused by the uniaxial stress are largest for the (111) case and smallest for the (001) case. The optical transition matrix elements change substantially after the crossover of the first heavy- and light-hole energy has occurred.

I. INTRODUCTION

Recently there has been increasing interest in superlattices grown on variously oriented substrates for both practical and theoretical reasons. The (11 N)-oriented growth of GaAs and Al $_x$ Ga $_{1-x}$ As arose within the context of the growth of these compound semiconductors on Si substrates. It has been shown that, for such polar-on-unipolar growth, the (110) and (112) orientations are the preferred growth orientation, leading to better nucleation and morphology than the traditional (001) orientation.¹⁻³ In addition, layers of some (11 N) GaAs of high quality grown by molecular-beam epitaxy (MBE) are also of importance for many potential applications, as they promise increased efficiency for electronic and optical devices.^{4,5}

To date, there have been many reports about successful growth of high-quality (11 N)-oriented GaAs/Al $_x$ Ga $_{1-x}$ As superlattices with excellent optical and electric properties, comparable to those with (001) orientation. Wang⁶ has reported that the surface morphology of (11 N) MBE GaAs/Al $_x$ Ga $_{1-x}$ As layers ($N=2, 3, 5, 7, 9$) is excellent and the two-dimensional carrier mobility in modulation-doped heterostructures grown on these high-index planes reaches $\sim 10^5$ cm²V⁻¹s⁻¹ (at 4 K), comparable to those grown on the (001) plane. Subbanna *et al.*⁷ observed that the photoluminescence (PL) intensities from the GaAs/Al $_x$ Ga $_{1-x}$ As superlattices grown on (112) $_A$ and (112) $_B$ substrates are significantly larger than those for the (001) structure, and the linewidth from (112) $_A$ seems to compare favorably with that from the (001) structure. Fukunaga *et al.*⁸ measured the PL spectra from GaAs-Al $_{0.24}$ Ga $_{0.76}$ As single quantum wells (SQW's) grown on (001), (113) $_A$, and (113) $_B$ substrates, and found that typical full widths at half maximum (FWHM's) of PL peaks are comparable for (001), (113) $_A$, and (113) $_B$ SQW's, indicating that the microscopic roughness in the (113) heterointerface is similar to that in

the (001) heterointerface. Allen *et al.*⁹ showed that the (110) layers exhibit a room-temperature electron mobility of 5700 cm²V⁻¹s⁻¹ for carrier concentration $n \sim 4 \times 10^{15}$ cm⁻² and a strong exciton PL emission at 4 K. Hayakawa *et al.*¹⁰ found that the PL efficiency of (111)-oriented quantum-well structure (QWS) is higher than the (001)-oriented QWS, and the threshold current density of (111)-oriented quantum-well lasers is less than the (001)-oriented ones. In addition, Hayakawa *et al.*,¹¹ Molenkamp *et al.*,¹² Bauer *et al.*,¹³ and Gil *et al.*¹⁴ investigated the variation of the binding energy of the 1s exciton for (001)-, (111)-, (110)-, (310)-, and (113)-oriented QWS's, and found that the binding energy of the light-hole exciton is more sensitive to the substrate orientation than that of the heavy-hole exciton. Khalifi *et al.*¹⁵ compared the splitting between first heavy-hole and light-hole subbands for the (113) $_B$ - and (001)-oriented GaAs/Al $_x$ Ga $_{1-x}$ As SQW's. Shanabrook *et al.*¹⁶ reported the observation of intersubband transitions of photoexcited holes in undoped multiple quantum wells (MQW's) grown in the [111] $_B$ and [001] directions with resonant electron Raman scattering. From the energies of intersubband transitions they determined another set of Luttinger effective-mass parameters¹⁷ γ_1 , γ_2 , and γ_3 .

That the valence band of GaAs near the Γ point is anisotropic can be seen in the ratio of the effective masses for the heavy hole in the [111] and [001] directions: $m_{\text{HH}}^*([111])/m_{\text{HH}}^*([001])=0.9/0.34=2.65$,¹⁰ or $0.75/0.34=2.21$.¹⁶ It is expected that many properties of superlattices and QWS's will depend on the growth orientation. But as of now there is no systematic theory describing the electronic structure of superlattices grown on variously oriented substrates, except for some works studying the superlattice grown in the particular directions (for example, Refs. 13 and 18).

This paper proposes an effective-mass formulation for the valence-band structure of semiconductor superlattices

grown on (11 N)-oriented substrates based on Luttinger's theory.¹⁷ By use of this theory, we studied and compared the hole subband structure, the effect of the uniaxial stress along the growth direction, and the optical transition matrix elements for superlattices grown on (110), (111), (112), (113), and (11 ∞) [i.e., (001)] -oriented substrates. Section II gives an effective-mass theory for superlattices on (11 N)-oriented substrates. Section III shows the hole subband structures and optical transition matrix elements for (11 N) ($N=0, 1, 2, 3$, and ∞) -oriented superlattices. In Sec. IV, the effect of uniaxial stress along the growth direction is discussed.

II. EFFECTIVE-MASS THEORY FOR SUPERLATTICES GROWN ON (11 N)-ORIENTED SUBSTRATES

Let the three axes (1,2,3) of our coordinate system be the following: the 3 axis along the growth direction, the 1 and 2 axes in the ($\bar{1}$ 10) plane, and the 2 axis in the [$\bar{1}$ 10] direction. The angle between the 3 axis and the X - Y plane is denoted by θ ; thus for θ varying from 0 to $\pi/2$ the growth surface perpendicular to the 3 axis changes from (110) in succession to (111), (112), (113), until (11 ∞), i.e., (001). Making the coordinate transform,

$$\begin{aligned} k_x &= \frac{\delta}{\sqrt{2}}k_1 - \frac{1}{\sqrt{2}}k_2 + \frac{c}{\sqrt{2}}k_3, \\ k_y &= \frac{\delta}{\sqrt{2}}k_1 + \frac{1}{\sqrt{2}}k_2 + \frac{c}{\sqrt{2}}k_3, \end{aligned} \quad (1)$$

$$\begin{aligned} k_z &= -ck_1 + \delta k_3; \\ J_x &= \frac{\delta}{\sqrt{2}}J_1 - \frac{1}{\sqrt{2}}J_2 + \frac{c}{\sqrt{2}}J_3, \\ J_y &= \frac{\delta}{\sqrt{2}}J_1 + \frac{1}{\sqrt{2}}J_2 + \frac{c}{\sqrt{2}}J_3, \\ J_z &= -cJ_1 + \delta J_3. \end{aligned} \quad (2)$$

Here, and in the following, we use δ and c to represent $\sin\theta$ and $\cos\theta$, respectively. Inserting Eqs. (1) and (2) into the Luttinger effective-mass Hamiltonian for hole states,¹⁷

$$\begin{aligned} H &= \frac{1}{2m_0} [(\gamma_1 + \frac{\delta}{2}\gamma_2)k^2 - 2\gamma_2(k_x^2J_x^2 + k_y^2J_y^2 + k_z^2J_z^2) \\ &\quad - 4\gamma_3(\{k_x, k_y\}\{J_x, J_y\} + \{k_y, k_z\}\{J_y, J_z\} \\ &\quad + \{k_z, k_x\}\{J_z, J_x\})], \end{aligned} \quad (3)$$

and using the representation for J_1 , J_2 , and J_3 in Eq. (57) of Ref. 17, we obtain the effective-mass Hamiltonian in the (1,2,3) coordinate system,

$$\begin{aligned} H &= \frac{1}{2m_0} [\gamma_1 k^2 + \gamma_2 (Ak_1^2 + Bk_2^2 + Ck_3^2 + Dk_1k_2 \\ &\quad + Ek_1k_3 + Fk_2k_3) \\ &\quad + \gamma_3 (A'k_1^2 + B'k_2^2 + C'k_3^2 + D'k_1k_2 \\ &\quad + E'k_1k_3 + F'k_2k_3)], \end{aligned} \quad (4)$$

where A, B, C, \dots, E', F' are 4×4 matrices with matrix elements as functions of δ and c , which all have the following form:

$$X = \begin{pmatrix} p & r & q & 0 \\ r^* & -p & 0 & -q \\ q^* & 0 & -p & r \\ 0 & -q^* & r^* & p \end{pmatrix}. \quad (5)$$

The values of p , r , and q for each matrix are given in Table I.

From Eqs. (4) and (5) and Table I, we can easily obtain the effective-mass Hamiltonian for any (11 N)-oriented superlattices, for example: $N=0$, $c=1$, $\delta=0$; $N=1$, $c=\sqrt{2}/3$, $\delta=1/\sqrt{3}$; $N=2$, $c=1/\sqrt{3}$, $\delta=\sqrt{2}/3$; $N=3$, $c=\sqrt{2}/11$, $\delta=3/\sqrt{11}$; $N=\infty$, $c=0$, $\delta=1$; etc. The Hamiltonian matrix has the following form:

$$H = \frac{1}{2m_0} \begin{pmatrix} P_1 & R & Q & 0 \\ R^* & P_2 & 0 & -Q \\ Q^* & 0 & P_2 & R \\ 0 & -Q^* & R^* & P_1 \end{pmatrix}, \quad (6)$$

where the P_1 and P_2 have the same forms, in which the γ_2 and γ_3 terms are of reverse signs. The P_1 , R , and Q in Eq. (6) for (11 N)-oriented ($N=0, 1, 2, 3$, and ∞) superlattices are given in Table II.

From Table II, we see that in the $N=\infty$ case the values of P_1 , R , and Q are just those for the (001) superlattice; for $k_1=k_2=0$, the off-diagonal elements vanish, and hence the hole effective-mass equation reduces to four independent equations with heavy- and light-effective mass $m_{\text{HH}}^* = m_0/(\gamma_1 - 2\gamma_2)$ and $m_{\text{LH}}^* = m_0/(\gamma_1 + 2\gamma_2)$, respectively. The case of $N=1$, i.e., (111) orientation is similar, but with the heavy- and light-hole effective mass $m_{\text{HH}}^* = m_0/(\gamma_1 - 2\gamma_3)$, and $m_{\text{LH}}^* = m_0/(\gamma_1 + 2\gamma_3)$, respectively. The other cases are more complicated: For $k_1=k_2=0$, the off-diagonal matrix elements $Q, R \neq 0$, and thus there is no simple effective mass to describe the movement of the heavy or light hole. From Table II we also see that the Hamiltonian is more complicated for larger N , i.e., high-index-substrate cases.

The hole motion equation in the superlattice can be written as

$$[H(k_1, k_2, k_3) + V(r_3)]\psi(\mathbf{r}) = E\psi(\mathbf{r}), \quad (7)$$

where the k_1 , k_2 , and k_3 in the Hamiltonian H [Eq. (6)] are operators $k_j = (1/i)(d/dr_j)$ ($j=1, 2, 3$). The growth direction of the superlattice is in the 3-axis direction, hence the effective potential V is only a function of r_3 . For the superlattice GaAs/Al $_x$ Ga $_{1-x}$ As the difference of the effective-mass parameters between the two materials is small; we can neglect the difference and use the continuity condition of wave functions instead of the particle-current conservation condition. We shall use the plane-wave expansion method^{19,20} to solve the effective-mass equation (7). Assume that the hole wave function has the form

TABLE I. Values of p , r , and q for matrices A, B, C, \dots, E', F' of Eq. (4). Here, as in text, the abbreviation $s \equiv \sin\theta$ and $c \equiv \cos\theta$ have been used.

	p	r	q
A	$\frac{3}{2}(\frac{2}{3} - 3c^2 + 3e^4)$	$\frac{\sqrt{3}}{2}e^2(1 - 3c^2)$	$\sqrt{3}sc(3c^2 - 1)$
B	$\frac{3}{2}(\frac{2}{3} - c^2)$	$\frac{\sqrt{3}}{2}e^2$	$-\sqrt{3}sc$
C	$\frac{3}{2}(-\frac{4}{3} + 4c^2 - 3e^4)$	$\frac{\sqrt{3}}{2}e^2(3c^2 - 2)$	$\sqrt{3}sc(2 - 3c^2)$
D	0	$i2\sqrt{3}s^2$	$i2\sqrt{3}sc$
E	$3sc(2 - 3c^2)$	$3\sqrt{3}sc^3$	$-6\sqrt{3}s^2e^2$
F	0	$i2\sqrt{3}sc$	$i2\sqrt{3}c^2$
A'	$\frac{9}{2}s^2e^2$	$-\frac{\sqrt{3}}{2}s^2(2 + 3c^2)$	$-\sqrt{3}sc(3c^2 - 1)$
B'	$\frac{3}{2}e^2$	$\frac{\sqrt{3}}{2}(2 - c^2)$	$\sqrt{3}sc$
C'	$-\frac{3}{2}e^2(4 - 3c^2)$	$-\frac{\sqrt{3}}{2}c^2(3c^2 - 2)$	$-\sqrt{3}sc(2 - 3c^2)$
D'	0	$i2\sqrt{3}c^2$	$-i2\sqrt{3}sc$
E'	$-3sc(2 - 3c^2)$	$-3\sqrt{3}sc^3$	$-2\sqrt{3}(3c^4 - 3c^2 + 1)$
F'	0	$-i2\sqrt{3}sc$	$i2\sqrt{3}s^2$

$$\psi_H(\mathbf{r}) = e^{i(k_1 r_1 + k_2 r_2)} \sum_n \begin{pmatrix} a_n \\ b_n \\ c_n \\ d_n \end{pmatrix} \frac{1}{\sqrt{L}} e^{i(k_3 + K_n)r_3}, \quad (8)$$

where $K_n = (2\pi/L)n$, $n = 0, \pm 1, \pm 2, \pm 3, \dots$, and L is the superlattice period; k_1 , k_2 , and k_3 are the wave-vector components of the hole, $-\pi/L < k_3 < \pi/L$. Inserting Eq. (8) into Eq. (7) we obtain a $4N \times 4N$ secular equation, where N is the number of K_n .

The conduction band is isotropic, independent of the

orientation, thus the electronic wave function in the superlattice can be written as

$$\psi_e(\mathbf{r}) = e^{i(k_1 r_1 + k_2 r_2)} \sum_n e_n \frac{1}{\sqrt{L}} e^{i(k_3 + K_n)r_3}. \quad (9)$$

The optical transition matrix elements²¹

$$Q_{ij}(\mathbf{k}_\parallel) = \frac{2}{m_0} |\hat{\mathbf{e}} \cdot \mathbf{P}_{ij}(\mathbf{k}_\parallel)|^2 \quad (10)$$

can be easily calculated by using Eqs. (8) and (9):

$$\begin{aligned} [Q_{ij}]_3 &= \left[\frac{2}{m_0} P^2 \right] \frac{2}{3} \left[\left(\sum_n e_n^* c_n \right)^2 + \left(\sum_n e_n^* b_n \right)^2 \right], \\ [Q_{ij}]_\parallel &= \left[\frac{2}{m_0} P^2 \right] \frac{1}{2} \left[\left(\sum_n e_n^* a_n \right)^2 + \left(\sum_n e_n^* d_n \right)^2 + \frac{1}{3} \left(\sum_n e_n^* b_n \right)^2 + \frac{1}{3} \left(\sum_n e_n^* c_n \right)^2 \right], \end{aligned} \quad (11)$$

where

$$P = \langle S | p_x | X \rangle = \langle S | p_y | Y \rangle = \langle S | p_z | Z \rangle.$$

$|S\rangle$ and $|X\rangle, |Y\rangle, |Z\rangle$ are orbital wave functions at the Γ point of the conduction band and valence band, respectively. $[Q_{ij}]_3$ and $[Q_{ij}]_\parallel$ are the optical transition matrix elements for light with polarization in the 3-axis direction and 1,2-axis direction (average), respectively. In deriving Eq. (11) we have summed the contribution from the electronic states [Eq. (9)] with up and down spins.

III. HOLE SUBBAND STRUCTURES AND OPTICAL TRANSITION MATRIX ELEMENTS FOR (11N)-ORIENTED GaAs/Al_{0.2}Ga_{0.8}As SUPERLATTICES

For comparison of hole subband structures and optical transition matrix elements for variously oriented GaAs/Al_{0.2}Ga_{0.8}As superlattices we calculate a special example with the following parameters: well width $L_w = 100$ Å, barrier width $L_b = 50$ Å, period $L = 150$ Å;

TABLE II. Values of P , R , and Q for the Hamiltonian matrix in Eq. (6) for $(11N)$ -oriented superlattices.

$N=0$	$P_1 = \gamma_1 k^2 + \frac{\gamma_2}{2}(2k_1^2 - k_2^2 - k_3^2) + \frac{3}{2}\gamma_3(k_2^2 - k_3^2)$ $R = \frac{\sqrt{3}}{2}[\gamma_2(-2k_1^2 + k_2^2 + k_3^2) + \gamma_3(k_2^2 - k_3^2 + 4ik_1k_2)]$ $Q = 2\sqrt{3}(\gamma_2 ik_2k_3 - \gamma_3 k_1k_3)$
$N=1$	$P_1 = (\gamma_1 + \gamma_3)k_{\parallel}^2 + (\gamma_1 - 2\gamma_3)k_3^2$ $R = -\frac{1}{\sqrt{3}}(\gamma_2 + 2\gamma_3)(k_1 - ik_2)^2 + \frac{2\sqrt{2}}{3}(\gamma_2 - \gamma_3)(k_1 + ik_2)k_3$ $Q = \sqrt{2/3}(\gamma_2 - \gamma_3)(k_1 + ik_2)^2 - \frac{2}{\sqrt{3}}(2\gamma_2 + \gamma_3)(k_1 - ik_2)k_3$
$N=2$	$P_1 = \gamma_1 k^2 + \frac{\gamma_2}{2}(k_2^2 - k_3^2 + 2\sqrt{2}k_1k_3) + \frac{\gamma_3}{2}(2k_1^2 + k_2^2 - 3k_3^2 - 2\sqrt{2}k_1k_3)$ $R = \frac{\gamma_2}{2\sqrt{3}}(k_2^2 - k_3^2 + 8ik_1k_2 + 2\sqrt{2}k_1k_3 + 4\sqrt{2}ik_2k_3)$ $+ \frac{\gamma_3}{2\sqrt{3}}(-6k_1^2 + 5k_2^2 + k_3^2 + 4ik_1k_2 - 2\sqrt{2}k_1k_3 - 4\sqrt{2}ik_2k_3)$ $Q = \sqrt{2/3}\gamma_2(-k_2^2 + k_3^2 + 2ik_1k_2 - 2\sqrt{2}k_1k_3 + \sqrt{2}ik_2k_3)$ $+ \sqrt{2/3}\gamma_3(k_2^2 - k_3^2 - 2ik_1k_2 - \sqrt{2}k_1k_3 + 2\sqrt{2}ik_2k_3)$
$N=3$	$P_1 = \gamma_1 k^2 + \frac{8}{121}\gamma_2(5k_1^2 + 11k_2^2 - 16k_3^2 + 18\sqrt{2}k_1k_3)$ $+ \frac{3}{121}\gamma_3(27k_1^2 + 11k_2^2 - 38k_3^2 - 48\sqrt{2}k_1k_3)$ $R = \frac{\sqrt{3}}{121}\gamma_2(5k_1^2 + 11k_2^2 - 16k_3^2 + 198ik_1k_2 + 18\sqrt{2}k_1k_3 + 66\sqrt{2}ik_2k_3)$ $- \frac{2\sqrt{3}}{121}\gamma_3(63k_1^2 - 55k_2^2 - 8k_3^2 - 22ik_1k_2 + 9\sqrt{2}k_1k_3 + 33\sqrt{2}ik_2k_3)$ $Q = \frac{\sqrt{6}}{121}\gamma_2(-15k_1^2 - 33k_2^2 + 48k_3^2 + 66ik_1k_2 - 54\sqrt{2}k_1k_3 + 22\sqrt{2}ik_2k_3)$ $+ \frac{\sqrt{6}}{121}\gamma_3(15k_1^2 + 33k_2^2 - 48k_3^2 - 66ik_1k_2 - 67\sqrt{2}k_1k_3 + 99\sqrt{2}ik_2k_3)$
$N=\infty$	$P_1 = (\gamma_1 + \gamma_2)k_{\parallel}^2 + (\gamma_1 - 2\gamma_2)k_3^2$ $R = 2\sqrt{3}i\gamma_2k_1k_2 - \sqrt{3}\gamma_3(k_1^2 - k_2^2)$ $Q = -2\sqrt{3}\gamma_3(k_1 - ik_2)k_3$

band offset $V_0 = 100$ meV for the valence band, $V_0 = 150$ meV for the conduction band; the valence-band effective-mass parameters $\gamma_1 = 6.85$, $\gamma_2 = 2.10$, and $\gamma_3 = 2.90$,²² and the conduction-band effective mass $m^* = 0.067m_0$.

We calculated the hole subbands along the k_1 and k_2 directions for GaAs/Al_{0.2}Ga_{0.8}As superlattices grown on $(11N)$ -oriented substrates with $N = \infty, 0, 1, 2$, and 3 , that for $n = \infty, 0, 1$ are shown in Figs. 1(a)–1(c), respectively.

$$E = \frac{1}{2m_0} \{ \gamma_1 k^2 \pm 2[\gamma_2^2 k^4 + 3(\gamma_3^2 - \gamma_2^2)(k_x^2 k_y^2 + k_y^2 k_z^2 + k_z^2 k_x^2)]^{1/2} \}. \quad (12)$$

Using the coordinate transform Eq. (1) we can transform Eq. (12) into the new coordinate system k_1, k_2, k_3 . Let $k_1 = k_2 = 0$, we obtain the energy dispersion along the k_3 direction, then the hole effective masses along the k_3

direction, Figure 1(a) is just that of the usual (001)-oriented superlattice. From Fig. 1 we see that the position and order of the heavy- and light-hole energy levels (denoted by HH and LH, respectively) are apparently different for various orientations, indicating the effect of anisotropy of the valence-band structure. In order to understand the variation trend of the hole subband we consider the classical energy-band model, in which the hole energy is given by

$$\left. \begin{array}{l} \text{direction,} \\ m_{\text{HH}}^* \\ m_{\text{LH}}^* \end{array} \right\} = m_0 \{ \gamma_1 \mp 2[\gamma_2^2 + \frac{3}{4}c^2(4 - 3c^2)(\gamma_3^2 - \gamma_2^2)]^{1/2} \}^{-1}, \quad (13)$$

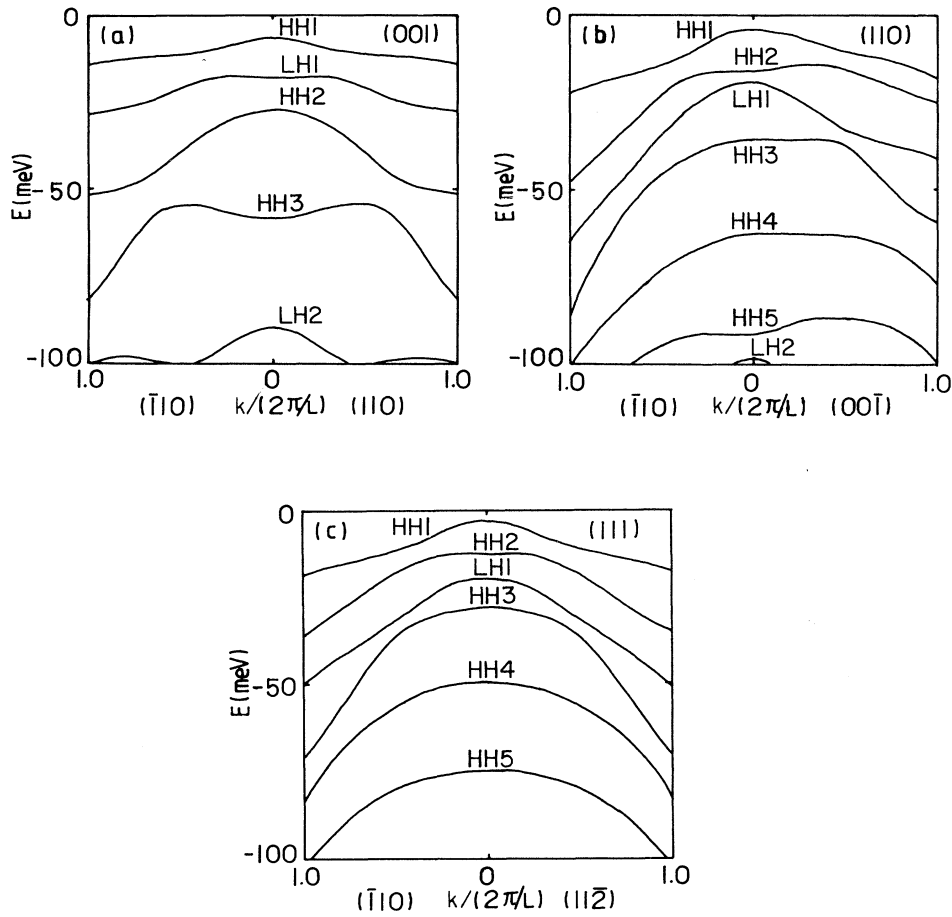


FIG. 1. Hole subband for superlattices grown on (11*N*)-oriented substrates with (a) $n = \infty$, (b) $N = 0$, (c) $N = 1$.

where the minus and plus signs correspond to the heavy and light holes, respectively. Figure 2 shows the effective masses of the heavy and light holes as a function of θ , in which the (001), (110), (111), etc., particular directions are indicated. From Fig. 2 we see that the anisotropy of the effective mass is large for the heavy hole, small for the light hole. The effective mass of the heavy hole along the [111] direction is largest, and that along the [001] direction is smallest, $m_{HH}^*([111])/m_{HH}^*([001]) = 2.52$. We found that the energy levels calculated separately with the classical effective masses of the heavy and light holes [Eq. (13)] are completely in agreement with that calculated with Eq. (7) for $k_{\parallel} = 0$. This result is surprising, because only in the cases of (001) and (111) orientation can Eq. (7) reduce into four independent equations with effective masses $m_0/(\gamma_1 \mp 2\gamma_2)$ and $m_0/(\gamma_1 \mp 2\gamma_3)$, respectively. In other cases, for $k_{\parallel} = 0$, Eq. (7) is still a coupled set of equations (see Table II), which has no direct connect with the classical effective mass. From Fig. 2 the variation of the hole subband with the orientation can be easily understood. For $k_{\parallel} = 0$, the first light-hole energy levels LH1 are basically unvaried due to the approximate constant of m_{LH}^* , while the variation of the LH2 levels is due to its closing to the barrier top. When the orienta-

tion changes from (001) to (113), (112), (111), the heavy-hole effective mass increases, hence the heavy-hole energy levels HH n at $k_{\parallel} = 0$ arise; in the (112) and (111) cases the HH2 energy level becomes higher than the LH1 energy

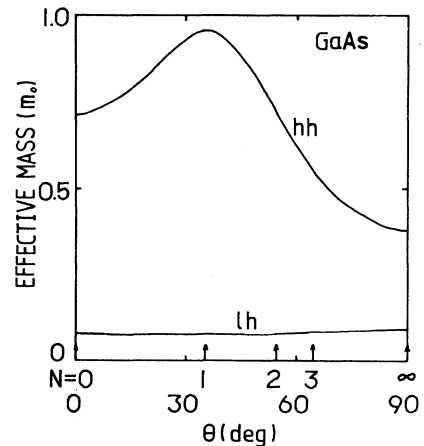


FIG. 2. Effective masses of the heavy hole (HH) and light hole (LH) as functions of θ .

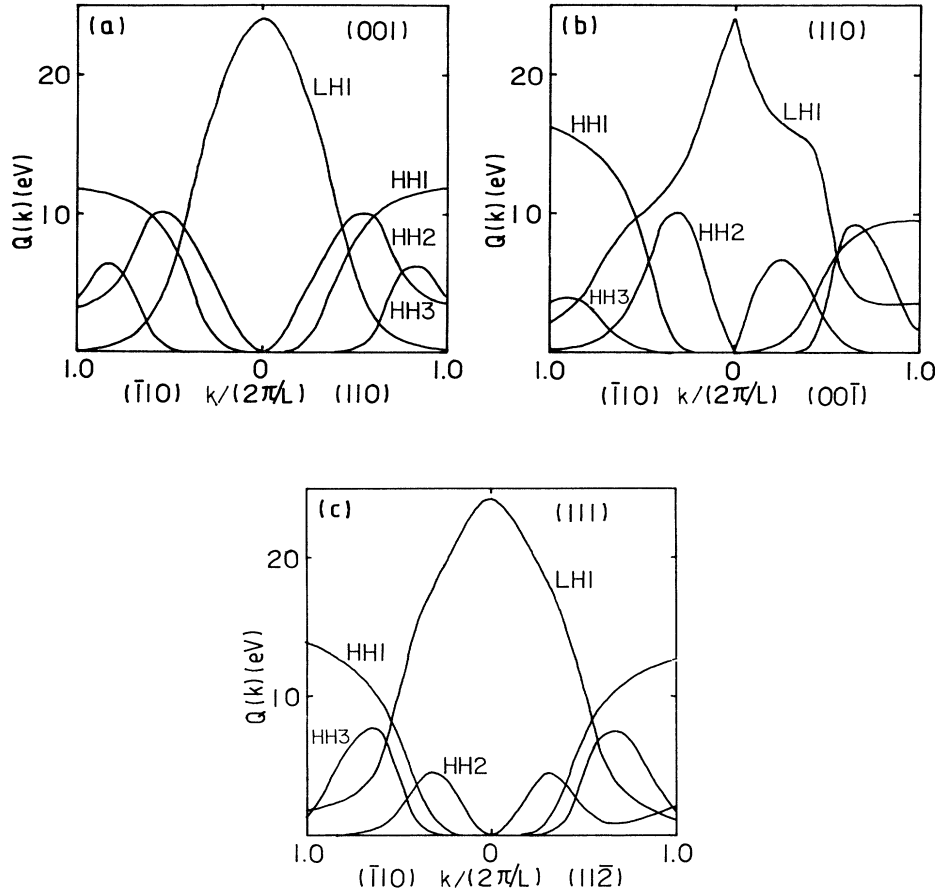


FIG. 3. Optical transition matrix elements $[Q_{ij}(\mathbf{k}_{\parallel})]_3$ from CB1 to hole states for $(11N)$ -oriented superlattices with (a) $N = \infty$, (b) $N = 0$, (c) $N = 1$.

level. The effective mass for the (110) case is equal to that of the (112) case [see Eq. (13)], so that the HH n energy levels at $\mathbf{k}_{\parallel} = 0$ are the same for the two cases. When $\mathbf{k}_{\parallel} \neq 0$, the hole subband dispersion along the k_1 and k_2 directions (perpendicular to each other) are symmetrical for the (001) and (111) cases, not symmetrical for the other cases, and the nonsymmetry is most obvious for the (110) case.

Figures 3(a)–3(c) and 4(a)–4(c) are the optical transition matrix elements $[Q_{ij}(\mathbf{k}_{\parallel})]_3$ and $[Q_{ij}(\mathbf{k}_{\parallel})]_{\parallel}$ from the first electronic energy level CB1 to the hole energy levels HH1, HH2, HH3, and LH1 for $(11N)$ -oriented superlattices with $N = \infty, 0, 1$, respectively. From the figures we see that in contrast with the energy-level position, the variation of the optical transition matrix elements with the orientation is more apparent for the light hole (especially CB1-LH1) than for the heavy hole. Because the coupling between the LH1 and HH2 states is sensitive to the orientation (see Fig. 1), the wave functions of the LH1 state greatly change as the orientation changes. It is expected that the binding energy of the light-hole exciton will vary with the orientation more obviously than that of the heavy-hole exciton.

IV. EFFECT OF UNIAXIAL STRESS ALONG THE GROWTH DIRECTION

The method applied in Sec. III can be extended to the cases of applied electric field, magnetic field, and stress, etc. For the case of applied magnetic field we only need to change the $k_1 k_2$ or $k_1 k_3$ terms in the Hamiltonian [Eq. (4) and Table I] into $\{k_1, k_2\}$ or $\{k_1, k_3\}$ terms, depending on the direction of the applied magnetic field parallel or perpendicular to the growth direction of the superlattice, respectively:

$$\{k_1, k_2\} = \frac{1}{2}(k_1 k_2 + k_2 k_1).$$

Besides, an $(e/c)\kappa\mathbf{J}\cdot\mathbf{H}$ term should be added to the Hamiltonian in Eq. (4).

Here we discuss the effect of uniaxial stress along the growth direction. The additional Hamiltonian caused by uniaxial stress is given by²³ (assuming the negative hole energy as positive)

$$\begin{aligned} H_S = & -D_d(\epsilon_{xx} + \epsilon_{yy} + \epsilon_{zz}) \\ & -\frac{2}{3}D_u[(J_x^2 - \frac{1}{3}J^2)\epsilon_{xx} + \text{c.p.}] \\ & -\frac{2}{3}D'_u[2\{J_x, J_y\}\epsilon_{xy} + \text{c.p.}], \end{aligned} \quad (14)$$

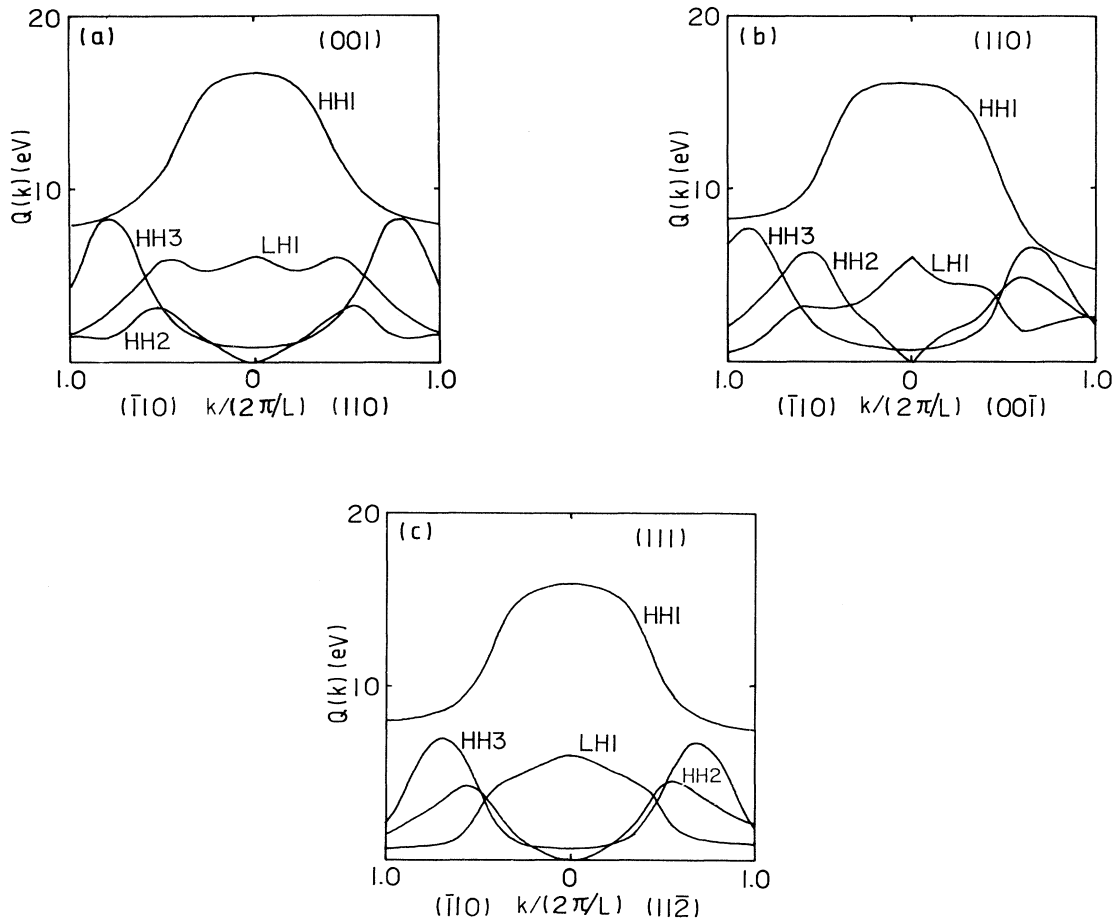


FIG. 4. Same as Fig. 3, but for $[Q_{ij}(\mathbf{k}_{\parallel})]_{\parallel}$.

where D_d, D_u, D'_u are the deformation potentials, $\epsilon_{xx}, \epsilon_{yy}, \dots$ are the strain tensor components, c.p. refers to terms obtained through cyclic permutation of indices. We assume that the uniaxial stress is applied in the 3-axis direction, then from Eq. (1) we obtain the stress tensor components,

$$T_{\alpha\beta} = \tau_{\alpha} \tau_{\beta} T, \quad \alpha, \beta = x, y, z, \quad (15)$$

$$\tau_x = \tau_y = \frac{c}{\sqrt{2}}, \quad \tau_z = s,$$

and the strain tensor components,

$$\epsilon_{xx} = [(S_{11} - S_{12})\tau_x^2 + S_{12}]T, \quad \text{c.p.}; \quad (16)$$

$$\epsilon_{xy} = \frac{1}{2}\tau_x \tau_y S_{44}T, \quad \text{c.p.};$$

where S_{11}, S_{12}, S_{44} are the cubic elastic compliance constants.

From Eq. (16) we obtain

$$\epsilon_{xx} + \epsilon_{yy} + \epsilon_{zz} = (S_{11} + 2S_{12})T, \quad (17)$$

independent of the orientation, i.e., the first term in the strain Hamiltonian Eq. (14) represents a constant energy shift, which will not be taken into account in the following. Using Eq. (16) the Hamiltonian Eq. (14) can be rewritten as

$$H_S = -\epsilon_u [(\mathbf{J} \cdot \boldsymbol{\tau})^2 - \frac{1}{3}J^2] + (\epsilon_u - \epsilon'_u)(2\{J_x, J_y\}\tau_x \tau_y + \text{c.p.}), \quad (18)$$

where

$$\epsilon_u = \frac{2}{3}D_u(S_{11} - S_{12})T, \quad (19)$$

$$\epsilon'_u = \frac{1}{3}D'_u S_{44}T.$$

Transforming J_x, J_y, J_z into the new coordinates J_1, J_2, J_3 , we obtain

$$H_S = -\epsilon_u (J_3^2 - \frac{s}{4}) - (\epsilon_u - \epsilon'_u) (\frac{3}{2}s^2 c^2 J_1^2 + (c^2/2)J_2^2 - [(c^4/2) + 2s^2 c^2]J_3^2 + sc(c^2 - 2s^2)\{J_1, J_3\}). \quad (20)$$

The second term in Eq. (20) can be written as a 4×4 matrix form,

$$(\epsilon_u' - \epsilon_u) \begin{pmatrix} t & v & u & 0 \\ v & -t & 0 & -u \\ u & 0 & -t & v \\ 0 & -u & v & t \end{pmatrix}, \quad (21)$$

where

$$\begin{aligned} t &= 3c^2(\frac{3}{4}c^2 - 1), \\ v &= \frac{\sqrt{3}}{4}c^2(2 - 3c^2), \\ u &= \frac{\sqrt{3}}{2}sc(3c^2 - 2). \end{aligned} \quad (22)$$

Taking the elastic compliance constants²⁴ $S_{11} = 1.150$, $S_{12} = -0.358$, $S_{44} = 1.657$ (10^{-3} kbar⁻¹), and deformation-potential parameters $\frac{2}{3}D_u = 1.71$ and $\frac{2}{3}D_u' = 4.55$ eV, we calculated the hole subbands for (11 \bar{N})-oriented superlattices under the uniaxial stress. The results for the (111) superlattice under the uniaxial stresses $T = 2.0$ and 2.5 kbar are shown in Fig. 5. From Fig. 5 we see that under a uniaxial stress along the growth direction the heavy- and light-hole energy levels shift down and up, respectively, and at a critical stress the HH1 and LH1 energy levels cross over, in agreement with the results of Ref. 25 for the (001) case. The energy shifts caused by the uniaxial stress are largest for the (111) orientation, smallest for the (001) orientation. The strain Hamiltonian Eq. (20) becomes $-\epsilon_u(J_3^2 - \frac{s}{4})$ and $-\epsilon_u'(J_3^2 - \frac{s}{4})$ for the (001) and (111) cases, respectively. According to the elastic and deformation-potential parameters of GaAs taken in this paper, $\epsilon_u'/\epsilon_u = 1.46$. It is noticed that at $\mathbf{k}_{\parallel} = 0$ the energy shifts are equal for the (110) and (112) cases. In Fig. 5 when the uniaxial stress (2.0 kbar) is just smaller than the critical stress there is a strong coupling between the HH1 and LH1 states for $\mathbf{k}_{\parallel} \neq 0$, resulting in an anticrossing of the HH1 and LH1 subbands near $|k_{\parallel}| = 0.2(2\pi/L)$; for the uniaxial stress

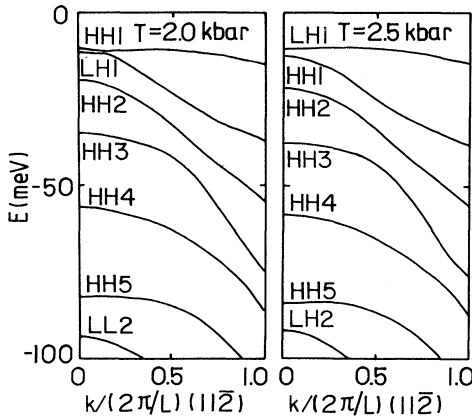


FIG. 5. Hole subband for (111)-oriented superlattices under the uniaxial stresses $T = 2.0$ and 2.5 kbar.

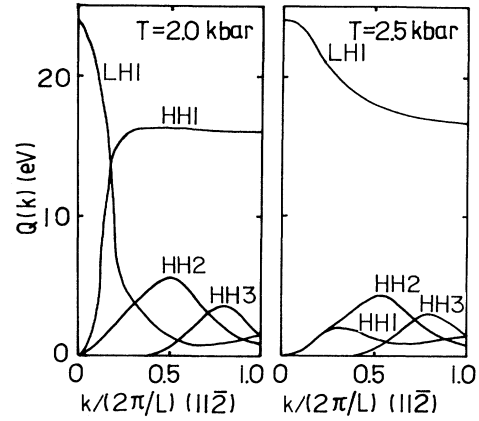


FIG. 6. Optical transition matrix elements $[Q_{ij}(\mathbf{k}_{\parallel})]_3$ from CB1 to hole states for the (111)-oriented superlattice under the uniaxial stresses $T = 2.0$ and 2.5 kbar.

(2.5 kbar) larger than the critical stress the coupling is weak, although the separation between the HH1 and LH1 states at $\mathbf{k}_{\parallel} = 0$ is small. This can be identified by the optical transition matrix elements.

The optical matrix elements $[Q_{ij}(\mathbf{k}_{\parallel})]_3$ and $[Q_{ij}(\mathbf{k}_{\parallel})]_{\parallel}$ for (11 \bar{N})-oriented superlattices under the uniaxial stress are calculated, that for the (111) case under the same uniaxial stresses as Fig. 5 are shown in Figs. 6 and 7, respectively. The $Q_{ij}(\mathbf{k}_{\parallel})$'s show an apparent difference for the uniaxial stresses just smaller and larger than the critical stress. In the former case the $[Q_{ij}(\mathbf{k}_{\parallel})]_3$ and $[Q_{ij}(\mathbf{k}_{\parallel})]_{\parallel}$ for the CB1-HH1 and CB1-LH1 transitions vary with k_{\parallel} dramatically due to the mixing of the HH1 and LH1 subbands. In the latter case the $[Q_{ij}(\mathbf{k}_{\parallel})]_3$ for the CB1-LH1 transition become rather flat, and those for CB1-HH n transitions become small. The $[Q_{ij}(\mathbf{k}_{\parallel})]_{\parallel}$ for the CB1-LH1 transition are also flat, and those for the CB1-HH1 transition decrease when k_{\parallel} increases, due to coupling with the HH2, HH3 states. It means that the coupling between the LH1 and HH1 subbands over the k_{\parallel} range considered is small.

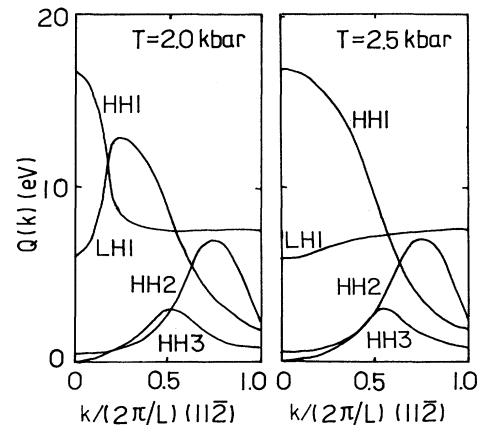


FIG. 7. Same as Fig. 6, but for $[Q_{ij}(\mathbf{k}_{\parallel})]_{\parallel}$.

V. SUMMARY

In this paper we have given an effective-mass formulation for superlattices grown on (11 \bar{N})-oriented substrates. It is found that for the GaAs/Al $_x$ Ga $_{1-x}$ As superlattice the hole subband structure and related properties are sensitive to the orientation, because of the large anisotropy of the valence band. The energy-level positions for the heavy hole and the optical transition matrix elements for the light hole apparently change with orientation. The heavy- and light-hole energy levels at $k_{\parallel}=0$ can be calculated separately by taking the classical effective mass in the k_3 direction. Under a uniaxial stress along the

growth direction the heavy- and light-hole energy levels shift down and up, respectively, and at a critical stress the LH1 and HH1 energy levels cross over. The energy shifts caused by the uniaxial stress are largest for the (111) case, smallest for the (001) case. The optical transition matrix elements change dramatically after the LH1 energy level crosses over the HH1 energy level.

ACKNOWLEDGMENTS

This work was supported by the Chinese National Science Foundation.

*Mailing address.

¹C. A. Chang, *Appl. Phys. Lett.* **40**, 1037 (1982).

²S. L. Wright, H. Kroemer, and M. Inada, *J. Appl. Phys.* **55**, 2916 (1984).

³P. N. Uppal and H. Kroemer, *J. Vac. Sci. Technol. B* **3**, 603 (1985).

⁴J. McKenna and F. K. Reinhart, *J. Appl. Phys.* **47**, 2069 (1976).

⁵T. P. Pearsall, F. Capasso, R. E. Nahory, M. A. Pollack, and J. R. Chelikowsky, *Solid-State Electron.* **21**, 297 (1978).

⁶W. I. Wang, *Surf. Sci.* **174**, 31 (1986).

⁷S. Subbanna, H. Kroemer, and J. L. Merz, *J. Appl. Phys.* **59**, 488 (1986).

⁸T. Fukunaga, T. Takamori, and H. Nakashima, *J. Cryst. Growth* **81**, 85 (1987).

⁹L. T. P. Allen, E. R. Weber, J. Washburn, and Y. C. Pao, *Appl. Phys. Lett.* **51**, 670 (1987).

¹⁰T. Hayakawa, K. Takahashi, M. Kondo, T. Suyama, S. Yamamoto, and T. Hijikata, *Phys. Rev. Lett.* **60**, 349 (1988).

¹¹T. Hayakawa, K. Takahashi, M. Kondo, T. Suyama, S. Yamamoto, and T. Hijikata, *Phys. Rev. B* **38**, 1526 (1988).

¹²L. M. Molenkamp, G. E. W. Bauer, R. Eppenga, and C. T. Foxon, *Phys. Rev. B* **38**, 6147 (1988).

¹³G. E. W. Bauer and T. Ando, *Phys. Rev. B* **38**, 6015 (1988).

¹⁴B. Gil, Y. El Khalifi, H. Mathieu, C. de Paris, J. Massies, G. Neu, T. Fukunaga, and H. Nakashima, *Phys. Rev. B* **41**, 2885 (1990).

¹⁵Y. El Khalifi, B. Gil, H. Mathieu, T. Fukunaga, and H. Nakashima, *Phys. Rev. B* **39**, 13 533 (1989).

¹⁶B. V. Shanabrook, O. J. Glembocki, D. A. Boido, and W. I. Wang, *Phys. Rev. B* **39**, 3411 (1989).

¹⁷J. M. Luttinger, *Phys. Rev.* **102**, 1030 (1956).

¹⁸C. Maihiot and D. L. Smith, *Phys. Rev. B* **35**, 1242 (1987).

¹⁹H. Tang and K. Huang, *Chin. J. Semicond.* **8**, 1 (1987).

²⁰K. Huang, J. B. Xia, B. F. Zhu and H. Tang, *J. Lumin.* **40&41**, 88 (1988).

²¹Y. C. Chang and J. N. Schulman, *Phys. Rev. B* **31**, 2069 (1985).

²²K. Hess, D. Bimberg, N. O. Lipari, J. U. Fischbach, and M. Altarelli, in *Proceedings of the Thirteenth International Conference on the Physics of Semiconductors, Rome, 1976*, edited by F. G. Fumi (North-Holland, Amsterdam, 1976), p. 142.

²³K. Suzuki and J. C. Hensel, *Phys. Rev. B* **9**, 4184 (1974).

²⁴D. Von Bimberg, in *Physics of Group IV Elements and III-IV Compounds*, edited by O. Madelung, Landolt-Börnstein, Vol. 17a (Springer-Verlag, Berlin, 1982).

²⁵G. D. Sanders and Y.-C. Chang, *Phys. Rev. B* **32**, 4282 (1985).